

# NanoGS: Training-Free Gaussian Splat Simplification

Butian Xiong<sup>1\*</sup>, Rong Liu<sup>1\*</sup>, Tiantian Zhou<sup>1</sup>,  
Meida Chen<sup>1</sup>, Zhiwen Fan<sup>2</sup>, and Andrew Feng<sup>1</sup>

<sup>1</sup> USC Institute for Creative Technologies

<sup>2</sup> Texas A&M University

17 Mar 2026

[cs.CV]

arXiv:2603.16103v1

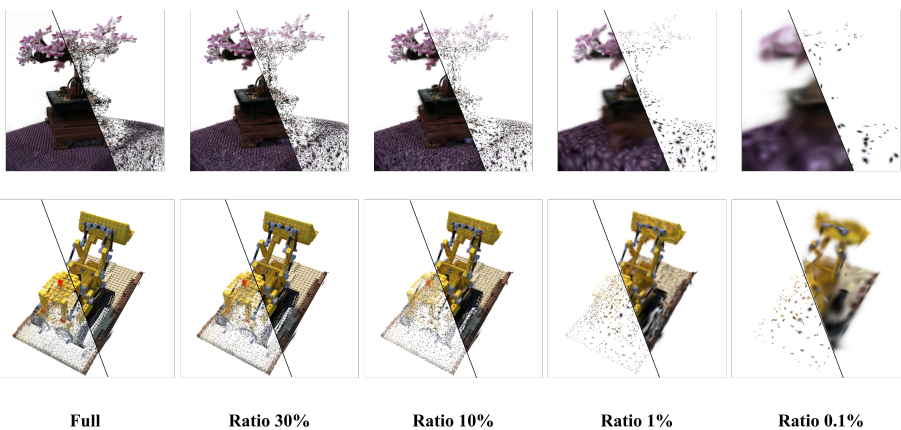


**Fig. 1:** NanoGS reduces Gaussian Splat primitive count from the full model to increasingly compact representations. NanoGS achieves substantial compaction ratio while preserving visual fidelity and geometric structure without GPU-intensive optimization or calibrated images.

**Abstract.** 3D Gaussian Splat (3DGS) enables high-fidelity, real-time novel view synthesis by representing scenes with large sets of anisotropic primitives, but often requires millions of Splats, incurring significant storage and transmission costs. Most existing compression methods rely on GPU-intensive post-training optimization with calibrated images, limiting practical deployment. We introduce **NanoGS**, a training-free and lightweight framework for Gaussian Splat simplification. Instead of relying on image-based rendering supervision, NanoGS formulates simplification as local pairwise merging over a sparse spatial graph. The method approximates a pair of Gaussians with a single primitive using mass preserved moment matching and evaluates merge quality through a principled merge cost between the original mixture and its approximation. By restricting merge candidates to local neighborhoods and

\* Co-first authors, equal technical contribution.

selecting compatible pairs efficiently, NanoGS produces compact Gaussian representations while preserving scene structure and appearance. NanoGS operates directly on existing Gaussian Splat models, runs efficiently on CPU, and preserves the standard 3DGS parameterization, enabling seamless integration with existing rendering pipelines. Experiments demonstrate that NanoGS substantially reduces primitive count while maintaining high rendering fidelity, providing an efficient and practical solution for Gaussian Splat simplification. Our project website is available at <https://saliteta.github.io/NanoGS/>.

## 1 Introduction

Real-time radiance field rendering has been fundamentally reshaped by 3D Gaussian Splatting (3DGS) [20]. By representing scenes as collections of anisotropic 3D Gaussians optimized with adaptive density control, 3DGS achieves photo-realistic novel view synthesis while sustaining real-time 1080p rendering performance. Its explicit, rasterization-compatible formulation bridges Neural Radiance Field (NeRF) [28] and classical graphics pipelines, eliminating costly volumetric ray sampling and enabling practical deployment. As a result, Splat-based representations have rapidly become a dominant alternative to NeRF-style models [4, 6, 28, 29], supporting applications in immersive exploration [14, 19], dynamic scene reconstruction [39, 41, 42], 3D content creation [35, 43], semantic distillation [33, 40, 47], and cinematic production [36].

Despite this success, a fundamental bottleneck persists: **scalability**, as high-fidelity reconstructions routinely require millions of primitives to capture fine geometric structures and complex view-dependent appearance. In practice, Splat models frequently occupy hundreds of megabytes or even gigabytes, while large primitive sets increase sorting and rasterization overhead during rendering. This structural scaling limits rendering speed, efficient transmission, edge-device deployment, and large-scale distribution of Splat-based content.

Existing methods mitigate this issue through optimization of the parameter dimensionality, quantization of attribute precision, and reduction of primitive counts [1, 2]. A large body of work focuses on parameter- and bit-level compression through vector quantization, entropy coding, adaptive spherical-harmonic reduction, structured parameter layouts, and progressive encoding schemes [13, 15, 23, 30, 31]. Other methods integrate pruning or sparsification into retraining pipelines, leveraging importance metrics, regularization, distillation, or optimal-transport-based merging to reduce the number of Splats [22, 37, 44]. However, these approaches often rely on GPU-intensive optimization and calibrated image supervision. This assumption does not hold in many practical scenarios where Splat models are produced through alternative pipelines, such as 3DGS generation [35, 43], edition [16, 32], or conversions from meshes or point clouds [12, 46], where guided images are not available. In addition, several compression schemes modify the underlying Gaussian Splat parameterization by introducing codec-specific layouts or structured representations, breaking compatibility with standard Splat rendering pipelines and preventing the compressed

models from being directly reused. Consequently, a training-free, lightweight, and representation-preserving simplification framework that operates *post hoc* on existing 3DGS models remains largely unexplored.

In this work, we introduce **NanoGS**, a training-free and lightweight framework for Gaussian Splat simplification. NanoGS operates directly in 3D space and formulates simplification as a local pairwise merging problem over a sparse spatial graph, avoiding image-based supervision. The method first removes visually insignificant splats through opacity pruning, then builds a sparse  $k$ -nearest neighbor graph to identify candidate merge pairs. For each pair, NanoGS evaluates a merge cost that measures how well the two-Gaussian mixture can be approximated by a single Gaussian via moment matching, capturing both geometric and appearance consistency. Low-cost disjoint pairs are greedily merged into new Gaussians whose parameters preserve the mass of the original pair, and the process repeats until the target simplification ratio is reached. Experiments show that NanoGS substantially reduces primitive count while maintaining high visual fidelity compared to state-of-the-art (SOTA) compression methods. Specifically, across four standard benchmarks (NeRF-Synthetic, Mip-NeRF 360, Tanks&Temples, Deep Blending; 21 scenes total) and three compaction budgets  $\rho \in \{0.1, 0.01, 0.001\}$ , NanoGS achieves the best PSNR at every budget and improves over the compared methods by **+2.40 dB**, **+4.84 dB**, and **+5.46 dB** on average, respectively. Importantly, NanoGS operates directly on existing Gaussian Splat models without requiring training images or optimization, enabling a lightweight post-processing step that preserves the standard Gaussian Splat representation and remains fully compatible with existing rendering pipelines.

In summary, our contributions are as follows:

1. **NanoGS**, a training-free and lightweight framework for simplifying Gaussian Splat representations directly in 3D space, avoiding rendering supervision and scene-specific optimization.
2. **Efficient graph pairing**, which restricts merge candidates to a sparse spatial neighborhood graph and selects disjoint low-cost pairs through greedy matching for scalable simplification.
3. **Mass Preserved Moment Matching**, a principled formulation that approximates two splats with a single Gaussian while preserving geometric and appearance consistency.
4. **I-divergence merge cost**, which scores candidate edges using a geometry term defined as the I-divergence between the two-splat mixture and its moment-matched Gaussian approximation, combined with an appearance feature discrepancy to guide robust merging.
5. **Accessible design**, which enables NanoGS to operate directly on existing 3DGS models, run efficiently on CPU, and remain fully compatible with standard Gaussian Splat rendering pipelines.

## 2 Related Works

Recent work has explored improving the efficiency of 3D Gaussian Splatting (3DGS) models along two complementary directions: *compression* and *compaction* [1, 2]. *Compression* methods aim to reduce the storage footprint and transmission bandwidth of 3DGS assets through efficient parameter representations and attribute quantization. In contrast, *compaction* methods focus on reducing the number of Gaussian primitives while preserving rendering quality, thereby lowering both memory consumption and rasterization cost during rendering. These two directions address different aspects of efficiency and are largely orthogonal: compression minimizes the bit-level storage of its parameters, while compaction simplifies the structural complexity of the representation.

### 2.1 3DGS Compression: Bit-Level Storage Reduction

While 3D Gaussian Splatting (3DGS) enables real-time photorealistic rendering, early models often produce serialized assets ranging from hundreds of megabytes to several gigabytes, creating a major bottleneck for storage, transmission, and web-based deployment [1, 8, 30]. To address this issue, a large body of work focuses on *bit-level compression* of Gaussian attributes. These methods typically quantize and entropy-code per-Gaussian parameters such as position, covariance, color coefficients, and opacity, often combined with learned or engineered context models and auxiliary coding structures, including anchor-based predictors and hierarchical entropy models [8, 9, 24, 30, 38].

Representative approaches include Compressed3DGS [30], which employs sensitivity-aware clustering and quantization-aware fine-tuning to achieve up to  $31\times$  compression while maintaining rendering quality, and provides a WebGPU-based renderer for efficient browser visualization. Other methods improve storage efficiency by reducing the *per-primitive parameter payload* through compact parameterizations or shared representations, such as reduced bases, codebooks, or alternative primitive formulations, sometimes combined with auxiliary pruning strategies for additional memory savings [10, 25, 26, 31]. Note that our method belongs to the compaction category, reducing the number of Gaussian primitives while preserving the standard 3DGS representation. As a result, it remains fully compatible with existing compression techniques, which can be applied on top of the compacted model to further reduce the overall storage footprint.

While these approaches significantly reduce the storage cost of 3DGS assets, many rely on access to the calibrated training images to optimize compression modules. This assumption does not always hold in practice, particularly when Gaussian Splat models are generated, edited, or converted through alternative pipelines where training images are not required. Moreover, several methods introduce codec-specific parameterizations or auxiliary structures that may limit direct compatibility with standard 3DGS rendering pipelines.

## 2.2 3DGS Compaction: Primitive-Level Count Reduction

While sharing the goal of reducing the number of Gaussian primitives, existing compaction approaches differ substantially in their operational requirements and optimization strategies.

**Training-based compaction.** A line of work incorporates primitive reduction directly into the 3DGS training pipeline so that the model converges to fewer splats or a constrained primitive budget [23, 27, 45]. These methods typically introduce additional mechanisms such as learned masking, compact parameterizations, or resource-aware training schedules. For example, Compact3DGS [23] integrates masking and compact representations into the optimization process, while Taming 3DGS [27] explicitly targets high-quality reconstruction under limited resource budgets by controlling training-time allocation. While effective when retraining is possible, such approaches require access to the original training pipeline and therefore cannot serve as drop-in simplification tools for arbitrary pre-trained 3DGS assets.

**Image-guided pruning.** Another dominant strategy estimates the importance of each Gaussian by measuring its contribution to rendered pixels in the training views. These methods typically require training images, camera poses, and differentiable rendering signals during the compaction process. Representative examples include LightGaussian and PUP 3D-GS [13, 17], which compute per-splat importance scores based on reconstruction sensitivity and employ prune-and-recover or prune-and-refine stages to maintain rendering quality under high pruning ratios. Although effective, such pipelines depend on rendering supervision and access to the training images, limiting their applicability when only the trained splat model is available. In contrast, our approach is *model-only* and operates directly on the Gaussian set without requiring training images or camera parameters.

**Model-only primitive reduction.** More closely related to our formulation are classical approaches for Gaussian mixture reduction and clustering based on distributional similarity measures, including Bregman divergences and information-theoretic co-clustering [3, 7, 11, 34]. These techniques provide principled tools for approximating a mixture of Gaussians with a smaller set while preserving key statistical properties. GHAP [37] is the most closely related work in the 3DGS literature: it formulates the geometry of a splat model as an unnormalized Gaussian mixture and performs blockwise reduction using an optimal-transport-based objective, followed by an appearance refinement stage. While effective, it relies on subsequent optimization to restore appearance quality.

In contrast, our method focuses on lightweight *post-hoc* simplification of trained splat sets. Rather than solving a transport problem, we employ an efficient local merging strategy that approximates pairs of Gaussians via moment matching, enabling training-free compaction that operates directly on existing models while preserving geometric and appearance consistency.

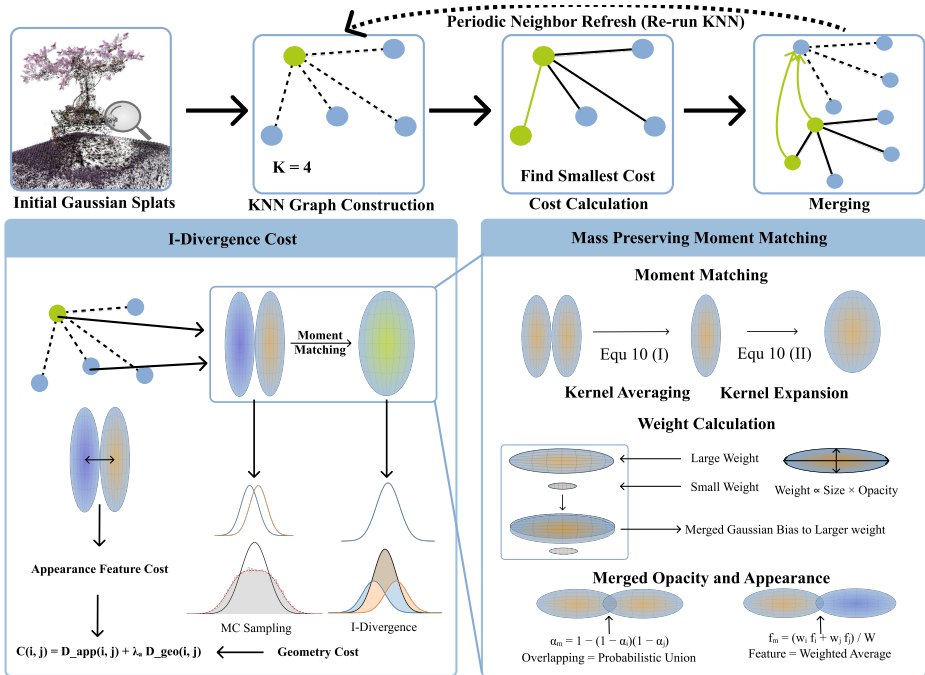


**Fig. 2: NanoGS pipeline overview.** (Top) Starting from an initial set of Gaussian splats, NanoGS constructs a sparse  $k$ -nearest-neighbor graph, evaluates a merge cost for each candidate edge, and collapses the lowest-cost disjoint pairs progressively. (Bottom-left) The merge cost combines an appearance term and a geometry term. The geometry cost measures the I-divergence between the original two-splat mixture and its single-Gaussian approximation. (Bottom-right) The Mass Preserved Moment Matching (MPMM) merge operator fuses a selected pair by computing mass-weighted moments, so the merged Gaussian is biased toward the larger primitive. Opacity is aggregated as a probabilistic union, and appearance features are blended as a weighted average.

### 3 Methods

In this section, we describe the proposed splat simplification framework built around a progressive graph-based merging pipeline. We first organize the unstructured splat set into a sparse  $k$ -nearest-neighbor (KNN) merge graph. The key idea is to turn an unstructured set of  $N$  splats into a sparse *merge graph* and then repeatedly collapse low-cost edges to construct a coarse-to-fine hierarchy of splat representations. Our pipeline comprises four modules: (i) **sparse merge-graph construction** (Sec. 3.1), (ii) **merge-cost evaluation** (Sec. 3.2), (iii) **a merge operator** that fuses a selected pair into one splat (Sec. 3.3), and (iv) **progressive batched edge collapses** with periodic neighborhood refresh to reach any target compression level (Sec. 3.4).

### 3.1 Sparse Merge Graph Construction

Our merge objective assigns a cost to any pair of splats, but evaluating all  $\binom{N}{2}$  pairs is prohibitive for large scenes. We therefore construct a sparse *merge graph*  $G = (V, E)$  that restricts candidates to spatially local neighbors, reducing candidate evaluation from  $\mathcal{O}(N^2)$  to  $\mathcal{O}(kN)$ . Figure 2 (top, second panel) illustrates this step: each node connects to its  $k$  nearest neighbors (dashed edges), forming the candidate set that we will score and prune.

**KNN neighborhood graph.** Let each current splat  $i \in V$  have center  $\mu_i \in \mathbb{R}^3$ . For each  $i$ , we query its  $k$  nearest neighbors in 3D and add undirected edges  $(i, j)$  to  $E$ . This yields  $|V| = N$  and  $|E| = \mathcal{O}(kN)$ , which keeps candidate merges local while making edge scoring tractable.

**What the graph represents.** Each node corresponds to a (possibly already merged) splat, and each edge is a *candidate merge*. The rest of the method operates on this graph: we score edges, pick a set of disjoint edges, merge them in parallel, and update the graph.

### 3.2 Merge Cost

Intuitively (Fig. 2, bottom-left),  $\mathcal{D}_{\text{merge}}$  is small when the two Gaussians overlap enough that a single Gaussian can cover them with little mass mismatch, and large when the pair is multi-modal (well-separated means), forcing the approximation to either miss probability mass or over-inflate. We define the cost of merging two splat sets  $i$  and  $j$  as a combination of a **geometric merge distortion** and an **appearance discrepancy**:

$$\mathcal{C}(i, j) = \mathcal{D}_{\text{geo}}(i, j) + \mathcal{D}_{\text{app}}(i, j), \quad (1)$$

**Geometry discrepancy = merge distortion.** For a candidate pair  $(i, j)$ , the geometric term measures the distortion incurred when replacing the two-splat mixture by a single merged splat:

$$\mathcal{D}_{\text{geo}}(i, j) \doteq \mathcal{D}_{\text{merge}}(i, j \rightarrow m), \quad (2)$$

where  $m$  denotes the merged splat produced by our merge operator (Sec. 3.3).

**Merge distortion (mixture  $\rightarrow$  Gaussian).** We regard each splat as an *unnormalized* Gaussian mass density

$$p_i(x) \doteq w_i \mathcal{N}(x; \mu_i, \Sigma_i), \quad w_i \doteq (2\pi)^{3/2} \alpha_i \prod_k s_{i,k}, \quad i \in \mathcal{S}, \quad (3)$$

where  $\mathcal{S}$  denotes the current splat set and  $\alpha_i \in [0, 1]$  is opacity. In Monte Carlo evaluation we draw  $S$  samples per candidate pair, with  $S$  a small fixed constant.

Let  $p_{ij}(x) = p_i(x) + p_j(x)$  denote the unnormalized mixture, and define the *normalized* mixture distribution

$$\tilde{p}_{ij}(x) \doteq \frac{p_{ij}(x)}{W} = \pi \mathcal{N}(x; \mu_i, \Sigma_i) + (1 - \pi) \mathcal{N}(x; \mu_j, \Sigma_j), \quad \pi \doteq \frac{w_i}{W}. \quad (4)$$

We approximate  $\tilde{p}_{ij}$  by the merged Gaussian  $q_m(x) = \mathcal{N}(x; \mu_m, \Sigma_m)$  produced by our VM moment matching, and define the merge distortion as the I-divergence

$$\mathcal{D}_{\text{merge}}(i, j \rightarrow m) \doteq \text{I}(\tilde{p}_{ij} \| q_m) = \int \tilde{p}_{ij}(x) \log \frac{\tilde{p}_{ij}(x)}{q_m(x)} dx. \quad (5)$$

Because the mixture term  $\log(\pi\mathcal{N}_i + (1 - \pi)\mathcal{N}_j)$  has no closed form, we estimate (5) with a small fixed number of Monte Carlo samples per candidate pair; details are provided in Appendix A.

**Appearance difference.** Each splat also carries an appearance feature vector  $f_i \in \mathbb{R}^F$  (e.g., spherical harmonics coefficients). We define the appearance discrepancy as the squared  $\ell_2$  distance:

$$\mathcal{D}_{\text{app}}(i, j) \doteq \|f_i - f_j\|_2^2. \quad (6)$$

### 3.3 Merging Operation

**Mass-preserving moment matching (MPMM).** Given a candidate pair of splats  $(i, j)$ , we construct a merged splat  $m$  by matching *mass-weighted* spatial moments and applying a saturating opacity composition. The key design choice is the weighting: rather than using opacity alone, we weight each splat by its *mass* (the integral of its normalized Gaussian density) so that splats with larger spatial extents and/or higher opacities contribute proportionally more to the merged moments. This is especially important under aggressive compression, where the remaining primitives must preserve coverage without collapsing toward small, high-variance outliers. This update has a direct geometric interpretation (Fig. 2, bottom-right): it consists of *kernel averaging* (preserving typical local shape) plus *kernel expansion* (inflating uncertainty to cover between-mean dispersion). We therefore define:

**Mass weights.** Interpreting each splat as an unnormalized Gaussian mass density, the mass of splat  $i$  is

$$w_i \doteq (2\pi)^{3/2} \alpha_i \prod_k s_{i,k}, \quad w_j \doteq (2\pi)^{3/2} \alpha_j \prod_k s_{j,k}, \quad W \doteq w_i + w_j. \quad (7)$$

Intuitively,  $w$  approximates the total mass  $\int p_i(x) dx$  of an unnormalized Gaussian, and thus increases with both *size* (scale) and *opacity*.

**Mass-matched moments.** The merged mean and appearance feature are mass-weighted averages:

$$\mu_m = \frac{w_i \mu_i + w_j \mu_j}{W}, \quad f_m \doteq \frac{w_i f_i + w_j f_j}{W}. \quad (8)$$

The merged covariance matches mass-weighted second moments:

$$\Sigma_m = \frac{w_i (\Sigma_i + (\mu_i - \mu_m)(\mu_i - \mu_m)^\top) + w_j (\Sigma_j + (\mu_j - \mu_m)(\mu_j - \mu_m)^\top)}{W}. \quad (9)$$

Equivalently, introducing  $\mathcal{K} \doteq \{i, j\}$  and  $W \doteq \sum_{k \in \mathcal{K}} w_k$ , we obtain

$$\Sigma_m = \underbrace{\frac{1}{W} \sum_{k \in \mathcal{K}} w_k \Sigma_k}_{\text{(I) mass-weighted covariance average}} + \underbrace{\frac{1}{W} \sum_{k \in \mathcal{K}} w_k (\mu_k - \mu_m)(\mu_k - \mu_m)^\top}_{\text{(II) dispersion term}}. \quad (10)$$

The first term preserves the average *within-splat* shape, while the second term captures *between-mean dispersion*, expanding the merged Gaussian so that it covers the union of the two components.

**Opacity and appearance aggregation.** We compose opacities using the Porter–Duff *source-over* (“over”) rule, equivalently multiplying transmittances  $T = 1 - \alpha$

$$\alpha_m \doteq 1 - (1 - \alpha_i)(1 - \alpha_j) = \alpha_i + \alpha_j - \alpha_i \alpha_j. \quad (11)$$

This prevents unbounded opacity growth while encouraging the merged splat to remain visually present in low-splat regimes. Intuitively, the aggregation is the probabilistic union of two independent coverage events.

We refer to this operator as **Mass Preserved Moment Matching (MPMM)**. Compared to classical moment matching and linear opacity conservation, MPMM biases merges toward *coverage* by accounting for splat volume, which empirically reduces holes and improves rendering stability under extreme compression.

### 3.4 Progressive Batched Merging

We perform simplification by repeatedly collapsing low-cost edges in the merge graph, analogous to edge-collapse procedures in mesh simplification.

**Batched non-overlapping edge collapses.** Given edge costs  $\mathcal{C}(i, j)$  on  $E$  (Eq. 1), each pass selects a set of *non-overlapping* low-cost edges (a matching) and merges all selected pairs in parallel using MPMM (Sec. 3.3). Collapsing edges produces a new splat set and a coarser graph. Iterating this process yields a hierarchy of representations from fine to coarse, and we can stop once we reach a target number of splats or target compression ratio.

**Local neighborhood refresh.** Merges change local geometry and density, so a fixed initial KNN graph can miss newly adjacent merge candidates. We therefore periodically refresh candidate edges by re-running KNN queries around newly formed splats (and/or their local neighborhoods). This preserves scalability while allowing newly relevant pairs to become eligible candidates, improving merge quality versus a fully fixed edge set. Additional implementation details and pseudocode are provided in Appendix B.

## 4 Experiments

We evaluate on four widely used 3DGS benchmarks spanning both synthetic and real captured scenes: NeRF-Synthetic [28] (8 scenes), Mip-NeRF 360 [5] (9 unbounded real-world scenes), Tanks and Temples [21] (2 large-scale real scenes),

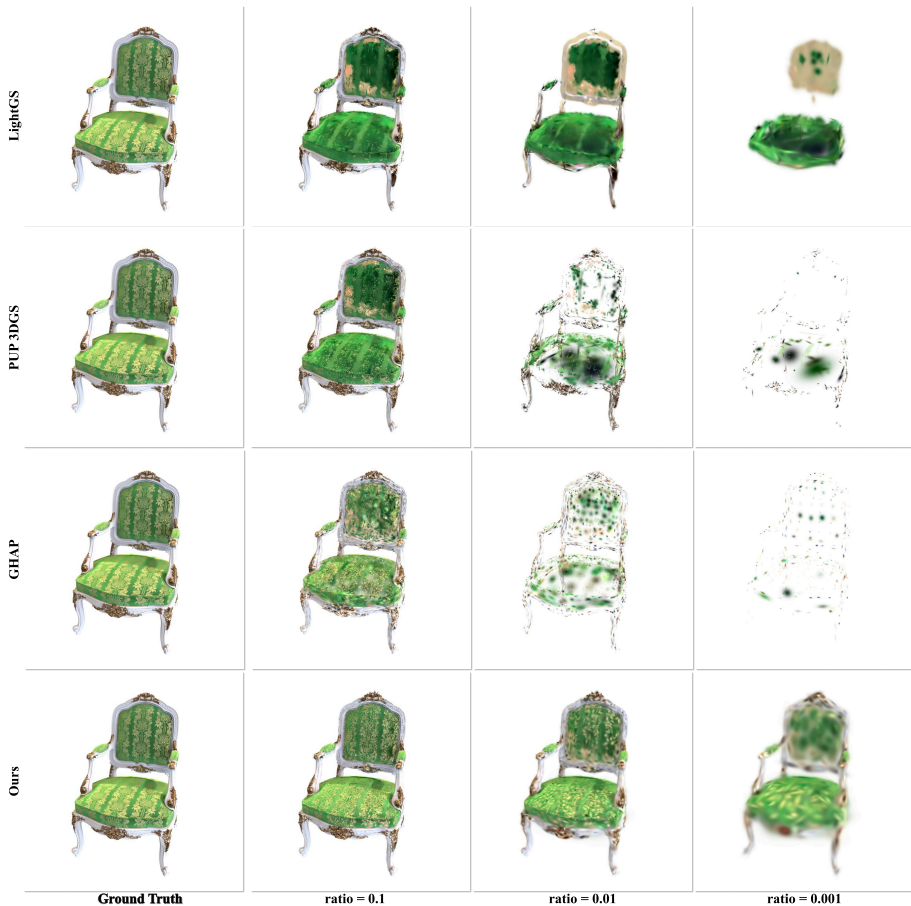


**Fig. 3: Qualitative comparison on chair from NeRF Synthetic dataset.** We show two representative test views. Columns correspond to the compaction ratio  $\rho \in \{0.1, 0.01, 0.001\}$  (leftmost: ground truth), and rows compare LightGS, PUP3DGS, GHAP, and Ours.

and Deep Blending [18] (2 challenging indoor scenes). This combination covers diverse geometry, appearance complexity, and camera trajectories.

**Evaluation Metrics.** We report Peak Signal-to-Noise Ratio (PSNR) and Structural Similarity Index Measure (SSIM) as primary visual fidelity metrics, and also report rendering speed (FPS) in Table 1. All metrics are computed on held-out test views following each benchmark’s standard evaluation protocol.

**Comparison Protocol.** Table 1 compares against LightGS [13], PUP3DGS [17], and GHAP [37]. Since our objective is *training-free* post-hoc compaction, we do not perform any post-compression fine-tuning. For methods that are typically paired with a fine-tuning stage (e.g., LightGS and PUP3DGS), we evaluate only their pruning/selection stage to isolate compaction quality. We report at three

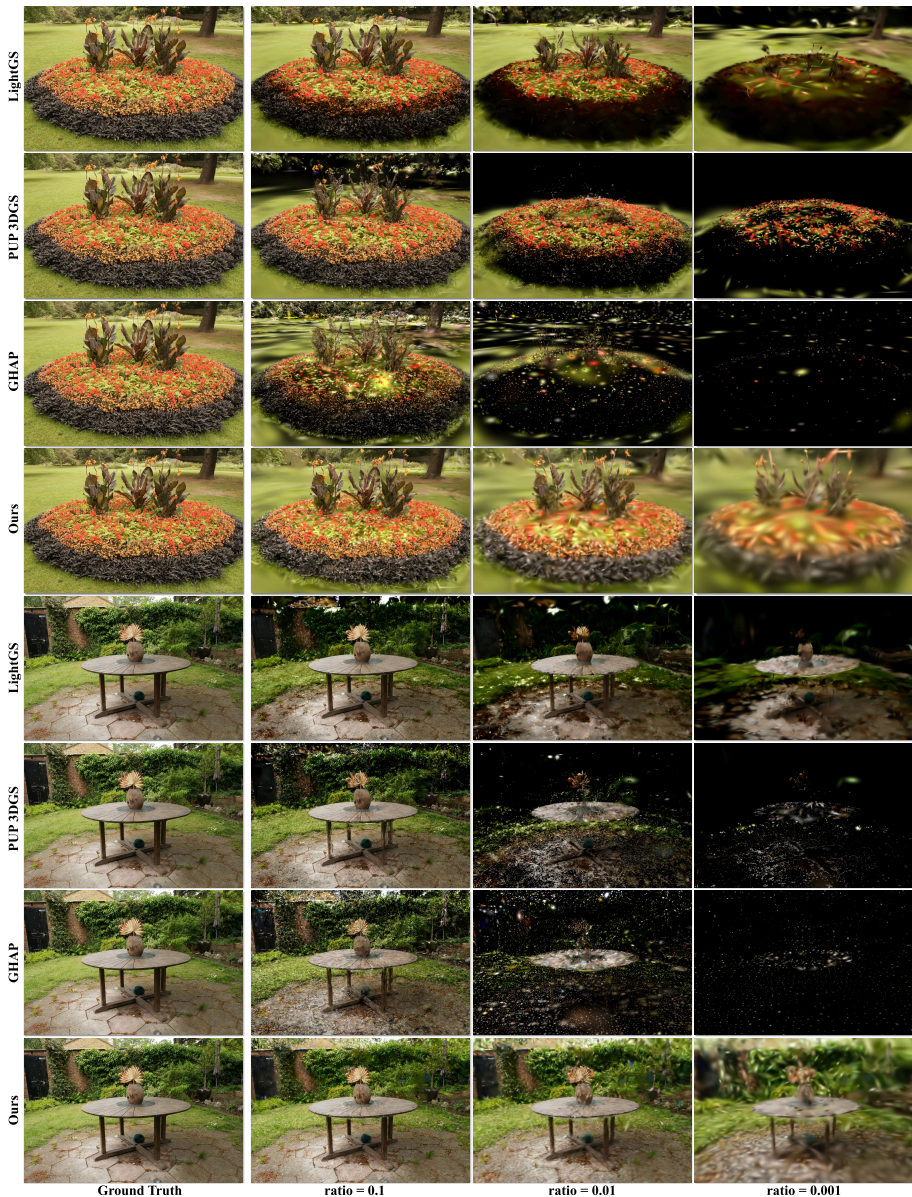


**Fig. 4: Qualitative comparison on Mip-NeRF 360 dataset.** We show two representative test views. Columns correspond to the compaction ratio  $\rho \in \{0.1, 0.01, 0.001\}$  (leftmost: ground truth), and rows compare LightGS, PUP3DGS, GHAP, and Ours.

Dataset (PSNR/SSIM/FPS) Full	Method	$\rho = 0.1$			$\rho = 0.01$			$\rho = 0.001$		
		PSNR	SSIM	FPS	PSNR	SSIM	FPS	PSNR	SSIM	FPS
NeRF Synth [28] 33.66/0.970/854.04	LightGS [13]	21.25	0.875	2204.97	15.76	0.807	2571.07	12.64	0.796	2623.73
	PUP3DGS [17]	20.24	0.860	2341.34	13.26	0.786	2676.07	11.31	0.792	2838.60
	GHAP [37]	20.09	0.838	2486.94	12.81	0.776	2679.19	11.07	0.791	2916.30
	Ours	25.81	0.910	2450.17	22.28	0.858	2598.03	19.04	0.822	2641.46
Mips-360 [4] 27.46/0.815/182.43	LightGS [13]	19.38	0.588	727.19	14.39	0.389	1525.92	11.97	0.278	2070.79
	PUP3DGS [17]	15.59	0.513	996.41	10.19	0.161	2407.68	8.81	0.056	2650.41
	GHAP [37]	17.35	0.444	1224.46	10.62	0.174	2557.02	8.52	0.035	2622.83
	Ours	21.97	0.582	1015.20	19.39	0.470	2005.76	17.20	0.430	2193.87
T&T [21] 23.63/0.847/299.07	LightGS [13]	17.50	0.642	1108.22	12.29	0.441	1995.98	9.36	0.341	2418.99
	PUP3DGS [17]	12.71	0.564	1283.38	8.22	0.266	2433.64	6.78	0.162	2593.01
	GHAP [37]	15.34	0.487	1665.64	8.43	0.220	2659.11	5.33	0.026	2670.40
	Ours	17.94	0.626	1429.88	15.29	0.501	2325.87	13.54	0.457	2487.31
D&B [18] 29.56/0.903/233.25	LightGS [13]	24.28	0.816	891.18	18.28	0.712	1878.64	13.41	0.616	2295.95
	PUP3DGS [17]	19.65	0.755	1325.03	8.83	0.282	2478.12	7.06	0.073	2672.21
	GHAP [37]	21.75	0.739	1375.59	11.36	0.435	2583.11	7.06	0.061	2627.05
	Ours	26.29	0.839	1202.23	23.12	0.780	2132.31	19.42	0.739	2321.92

**Table 1:** Quantitative benchmarks across datasets and sampling ratios  $\rho$ . Full-quality references (PSNR/SSIM/FPS at  $\rho = 1.0$ ) are listed in the Dataset column. For  $\rho \in \{0.1, 0.01, 0.001\}$ , color indicates rank within each dataset/metric column: red =1st, pink =2nd, yellow =3rd.

representative budgets,  $\rho \in \{0.1, 0.01, 0.001\}$ :  $\rho = 0.1$  follows the common GHAP setting, while  $\rho = 0.01$  and  $\rho = 0.001$  reflect more aggressive LOD-style compression.

**Implementation Details.** Our method operates directly on pretrained 3DGS assets and preserves the original 3DGS representation, so compressed outputs remain compatible with standard Gaussian splatting renderers. Unless otherwise noted, all experiments are conducted on a single NVIDIA RTX 4090 GPU with CUDA 12.8, and FPS is also measured on the same machine for fair comparison. We use a unified rendering/evaluation configuration across methods and report final results at each target ratio without additional retraining.

#### 4.1 Comparison with the State of the Art

Qualitatively, Fig. 4 and Fig. 3 mirrors the quantitative trend in Table 1. At moderate compression ( $\rho = 0.1$ ), all methods are broadly faithful. As the budget decreases ( $\rho = 0.01$  and  $0.001$ ), baselines increasingly collapse into sparse high-intensity splats and lose coherent surfaces, consistent with unstable merges and floater-dominated candidates. In contrast, our filtering and mass-preserving moment matching maintain more contiguous coverage and suppress isolated artifacts, leading to a more graceful degradation under extreme compaction. Additional qualitative comparison will be provided in appendix.

Table 1 compares our training-free post-hoc compaction against LightGS [13], PUP3DGS [17], and GHAP [37] at three representative budgets where  $\rho$  is the

compaction ratio  $\rho \in \{0.1, 0.01, 0.001\}$ . Across all four benchmarks, our method consistently achieves the best PSNR at every budget, and its advantage widens substantially as compression becomes more aggressive. Averaged over datasets, our PSNR improves over the best baseline by **+2.40 dB** at  $\rho=0.1$ , **+4.84 dB** at  $\rho=0.01$ , and **+5.46 dB** at  $\rho=0.001$ .

- *NeRF Synthetic (8 scenes)*. We achieve the largest gains on synthetic scenes: **25.81/0.910** at  $\rho=0.1$ , **22.28/0.858** at  $\rho=0.01$ , and **19.04/0.822** at  $\rho=0.001$ , outperforming the best baseline by **+4.56**, **+6.52**, and **+6.40** dB PSNR, respectively.
- *Mip-NeRF 360 (9 unbounded real scenes)*. We maintain a clear PSNR lead that widens at low budgets: **+2.59 dB** at  $\rho=0.1$  (SSIM comparable), **+5.00 dB / +0.081 SSIM** at  $\rho=0.01$ , and **+5.23 dB / +0.152 SSIM** at  $\rho=0.001$ .
- *Tanks & Temples (2 large-scale real scenes)*. Gains grow with compression: modest at  $\rho=0.1$  (**+0.44 dB**), then **+3.00 dB / +0.060 SSIM** at  $\rho=0.01$  and **+4.18 dB / +0.116 SSIM** at  $\rho=0.001$ , indicating fewer missing-geometry failures.
- *Deep Blending (2 indoor real scenes)*. We consistently improve quality across all budgets: **+2.01 dB / +0.023 SSIM** at  $\rho=0.1$ , **+4.84 dB / +0.068 SSIM** at  $\rho=0.01$ , and **+6.01 dB / +0.123 SSIM** at  $\rho=0.001$ .

Overall, the trend across datasets is consistent: baselines degrade rapidly as  $\rho$  decreases, while our merge-graph pipeline and mass-preserving moment matching maintain substantially higher fidelity, with the largest gains appearing in the most aggressive settings ( $\rho=0.01, 0.001$ ).

## 4.2 Ablation Study

Table 2 evaluates four variants of our training-free compaction: **w/o KNN graph** replaces KNN-graph-based candidate selection with an Octree-based neighborhood selection, **w/o filtering** disables the initial opacity-based pruning, **w/o I-divergence** replaces the I-divergence geometric term with a fast Mean Squared Error (MSE) surrogate, and **Full** uses the complete formulation.

**Candidate selection.** Replacing the KNN-graph candidate construction with Octree-based selection leads to a clear quality drop, especially at aggressive budgets. For example, on Mip-NeRF 360 at  $\rho=0.001$ , PSNR drops from **17.20** (Full) to **14.11** (w/o KNN graph), and on NeRF-Synthetic it drops from **19.04** to **15.85**. This indicates that KNN-graph locality provides more reliable merge candidates than the Octree alternative in our setting.

**Opacity filtering.** Removing filtering consistently hurts performance, particularly on Mip-NeRF 360. At  $\rho=0.001$ , PSNR drops from **17.20** (Full) to **14.67** (w/o filtering), while NeRF-Synthetic is less sensitive. This suggests that filtering suppresses low-opacity “floaters” that are commonly produced in real-world reconstructions.

**Merge cost.** Replacing the I-divergence geometric distortion with the fast surrogate consistently degrades reconstruction quality across both datasets and

Dataset	Method	$\rho = 0.1$		$\rho = 0.01$		$\rho = 0.001$	
		PSNR	SSIM	PSNR	SSIM	PSNR	SSIM
NeRF	w/o KNN graph	25.53	0.905	20.74	0.839	15.85	0.800
	w/o filtering	24.99	0.904	22.01	<b>0.858</b>	18.87	<b>0.822</b>
	w/o I-divergence	25.65	0.908	22.15	0.854	18.80	0.819
	Full	<b>25.81</b>	<b>0.910</b>	<b>22.28</b>	<b>0.858</b>	<b>19.04</b>	<b>0.822</b>
M360	w/o KNN graph	21.53	0.537	17.82	0.444	14.11	0.382
	w/o filtering	18.24	0.504	15.47	0.421	14.67	0.401
	w/o I-divergence	21.61	0.566	19.19	0.467	16.98	0.426
	Full	<b>21.97</b>	<b>0.582</b>	<b>19.39</b>	<b>0.470</b>	<b>17.20</b>	<b>0.430</b>

**Table 2:** Ablation study across datasets and compaction ratios. **w/o KNN graph** replaces the KNN-graph candidate selection with the Octree-based one; **w/o filtering** disables opacity-based filtering; **w/o I-divergence** replaces the principled I-divergence geometric cost with an Mean Squared Error surrogate; **Full** uses the complete proposed formulation. Bold indicates the best result within each dataset/metric column.

all compression ratios, indicating that the principled I-divergence formulation provides a more faithful geometric fidelity measure than the MSE-based approximation.

In sum, the ablation indicates that KNN-graph candidate selection improves merge reliability, filtering removes noisy floaters in the early stage, and the I-divergence cost provides additional geometry-aware guidance for selecting merges.

## 5 Conclusion

We presented **NanoGS**, a training-free and lightweight framework for Gaussian Splat simplification that operates directly on pretrained 3DGS models without requiring calibrated images or scene-specific optimization. By formulating simplification as progressive local pairwise merging over a sparse  $k$ -nearest-neighbor graph, NanoGS avoids the GPU-intensive retraining pipelines that limit the practical applicability of existing compaction methods. At the core of our approach is the Mass-Preserving Moment Matching (MPMM) operator, which fuses pairs of splats by matching mass-weighted spatial moments and compositing opacity as a probabilistic union, ensuring that merged primitives faithfully preserve spatial coverage and appearance. Across four standard benchmarks and varying compression budgets, NanoGS consistently outperforms state-of-the-art compaction methods, improving average PSNR by up to +5.46 dB at the most aggressive settings, with particularly stable degradation behavior at extreme ratios where prior methods collapse into floater-dominated artifacts.

**Future Work** Several directions remain open for future work. First, while NanoGS currently runs on CPU and preserves the standard 3DGS parameterization, a GPU-accelerated implementation of the graph construction and edge-collapse stages could substantially reduce wall-clock time for large-scale scenes.

Second, the merge cost and MPMM operator treat geometry and appearance independently; a jointly learned or view-dependent merge criterion could better capture perceptually important splats. Finally, the current method assumes the static environment. Extending the framework to dynamic 3DGS representations is a natural and practically important next step.

## References

1. Ali, M.S., Zhang, C., Cagnazzo, M., Valenzise, G., Tartaglione, E., Bae, S.H.: Compression in 3d gaussian splatting: A survey of methods, trends, and future directions. arXiv preprint arXiv:2502.19457 (2025)
2. Bagdasarian, M.T., Knoll, P., Li, Y., Barthel, F., Hilsmann, A., Eisert, P., Morgenstern, W.: 3dgs.zip: A survey on 3d gaussian splatting compression methods. *Computer Graphics Forum* (2025)
3. Banerjee, A., Merugu, S., Dhillon, I.S., Ghosh, J.: Clustering with bregman divergences. *Journal of machine learning research* **6**(Oct), 1705–1749 (2005)
4. Barron, J.T., Mildenhall, B., Tancik, M., Hedman, P., Martin-Brualla, R., Srinivasan, P.P.: Mip-nerf: A multiscale representation for anti-aliasing neural radiance fields. In: *CVPR* (2022)
5. Barron, J.T., Mildenhall, B., Verbin, D., Srinivasan, P.P., Hedman, P.: Mip-nerf 360: Unbounded anti-aliased neural radiance fields. In: *Proceedings of the IEEE/CVF conference on computer vision and pattern recognition*. pp. 5470–5479 (2022)
6. Barron, J.T., Mildenhall, B., Verbin, D., Srinivasan, P.P., Hedman, P.: Zip-nerf: Anti-aliased grid-based neural radiance fields. In: *ICCV* (2023)
7. Bregman, L.M.: The relaxation method of finding the common point of convex sets and its application to the solution of problems in convex programming. *USSR computational mathematics and mathematical physics* **7**(3), 200–217 (1967)
8. Chen, Y., Wu, Q., Lin, W., Harandi, M., Cai, J.: Hac: Hash-grid assisted context for 3d gaussian splatting compression. In: *European Conference on Computer Vision*. Springer (2024)
9. Chen, Y., Wu, Q., Lin, W., Harandi, M., Cai, J.: Hac++: Towards 100x compression of 3d gaussian splatting. arXiv preprint arXiv:2501.12255 (2025)
10. Deng, T., Chen, Y., Zhang, L., Yang, J., Yuan, S., Liu, J., Wang, D., Wang, H., Chen, W.: Compact 3d gaussian splatting for dense visual slam. arXiv preprint arXiv:2403.11247 (2024)
11. Dhillon, I.S., Mallela, S., Modha, D.S.: Information-theoretic co-clustering. In: *Proceedings of the ninth ACM SIGKDD international conference on Knowledge discovery and data mining*. pp. 89–98 (2003)
12. electronicarts: mesh2splat: Fast mesh to 3d gaussian splat conversion (2025), <https://github.com/electronicarts/mesh2splat>
13. Fan, Z., Wang, K., Wen, K., Zhu, Z., Xu, D., Wang, Z., et al.: Lightgaussian: Unbounded 3d gaussian compression with 15x reduction and 200+ fps. *Advances in neural information processing systems* **37**, 140138–140158 (2024)
14. Franke, L., Fink, L., Stamminger, M.: Vr-splatting: Foveated radiance field rendering via 3d gaussian splatting and neural points. *Proc. ACM Comput. Graph. Interact. Tech.* (2025)
15. Girish, S., Gupta, K., Shrivastava, A.: Eagles: Efficient accelerated 3d gaussians with lightweight encodings. In: *European Conference on Computer Vision*. pp. 54–71. Springer (2024)

16. Guédon, A., Lepetit, V.: Gaussian frosting: Editable complex radiance fields with real-time rendering. *ECCV* (2024)
17. Hanson, A., Tu, A., Singla, V., Jayawardhana, M., Zwicker, M., Goldstein, T.: Pup 3d-gs: Principled uncertainty pruning for 3d gaussian splatting. In: *Proceedings of the Computer Vision and Pattern Recognition Conference*. pp. 5949–5958 (2025)
18. Hedman, P., Philip, J., Price, T., Frahm, J.M., Drettakis, G., Brostow, G.: Deep blending for free-viewpoint image-based rendering. *ACM Transactions on Graphics (ToG)* **37**(6), 1–15 (2018)
19. Jiang, Y., Yu, C., Xie, T., Li, X., Feng, Y., Wang, H., Li, M., Lau, H., Gao, F., Yang, Y., Jiang, C.: Vr-gs: A physical dynamics-aware interactive gaussian splatting system in virtual reality. In: *SIGGRAPH* (2024)
20. Kerbl, B., Kopanas, G., Leimkühler, T., Drettakis, G.: 3d gaussian splatting for real-time radiance field rendering. In: *SIGGRAPH* (2023)
21. Knapitsch, A., Park, J., Zhou, Q.Y., Koltun, V.: Tanks and temples: Benchmarking large-scale scene reconstruction. *ACM Transactions on Graphics (ToG)* **36**(4), 1–13 (2017)
22. Lee, J.C., Ko, J.H., Park, E.: Optimized minimal 3d gaussian splatting (2025), <https://arxiv.org/abs/2503.16924>
23. Lee, J.C., Rho, D., Sun, X., Ko, J.H., Park, E.: Compact 3d gaussian representation for radiance field. In: *Proceedings of the IEEE/CVF Conference on Computer Vision and Pattern Recognition*. pp. 21719–21728 (2024)
24. Liu, L., Chen, Z., Jiang, W., Wang, W., Xu, D.: Hemgs: A hybrid entropy model for 3d gaussian splatting data compression. *arXiv preprint arXiv:2411.18473* (2024)
25. Liu, R., Gao, Z., Planche, B., Chen, M., Nguyen, V.N., Zheng, M., Choudhuri, A., Chen, T., Wang, Y., Feng, A., et al.: Universal beta splatting. *arXiv preprint arXiv:2510.03312* (2025)
26. Liu, R., Sun, D., Chen, M., Wang, Y., Feng, A.: Deformable beta splatting. In: *Proceedings of the Special Interest Group on Computer Graphics and Interactive Techniques Conference Conference Papers*. pp. 1–11 (2025)
27. Mallick, S.S., Goel, R., Kerbl, B., Steinberger, M., Carrasco, F.V., De La Torre, F.: Taming 3dgs: High-quality radiance fields with limited resources. In: *SIGGRAPH Asia 2024 Conference Papers*. pp. 1–11 (2024)
28. Mildenhall, B., Srinivasan, P.P., Tancik, M., Barron, J.T., Ramamoorthi, R., Ng, R.: Nerf: Representing scenes as neural radiance fields for view synthesis. In: *ECCV* (2020)
29. Müller, T., Evans, A., Schied, C., Keller, A.: Instant neural graphics primitives with a multiresolution hash encoding. In: *SIGGRAPH* (2022)
30. Niedermayr, S., Stumpfegger, J., Westermann, R.: Compressed 3d gaussian splatting for accelerated novel view synthesis. In: *Proceedings of the IEEE/CVF Conference on Computer Vision and Pattern Recognition*. pp. 10349–10358 (2024)
31. Papantonakis, P., Kopanas, G., Kerbl, B., Lanvin, A., Drettakis, G.: Reducing the memory footprint of 3d gaussian splatting. *Proceedings of the ACM on Computer Graphics and Interactive Techniques* **7**(1) (May 2024)
32. PlayCanvas: Supersplat: 3d gaussian splat editor (2024), <https://github.com/playcanvas/supersplat>
33. Qin, M., Li, W., Zhou, J., Wang, H., Pfister, H.: Langsplat: 3d language gaussian splatting. In: *Proceedings of the IEEE/CVF Conference on Computer Vision and Pattern Recognition*. pp. 20051–20060 (2024)
34. Runnalls, A.R.: Kullback-leibler approach to gaussian mixture reduction. *IEEE Transactions on Aerospace and Electronic Systems* **43**(3), 989–999 (2007)

35. Tang, J., Ren, J., Zhou, H., Liu, Z., Zeng, G.: Dreamgaussian: Generative gaussian splatting for efficient 3d content creation. In: ICLR (2024)
36. Wang, C., Wolski, K., Kerbl, B., Serrano, A., Bermana, M., Seidel, H.P., Myszkowski, K., Leimkühler, T.: Cinematic gaussians: Real-time hdr radiance fields with depth of field. In: Computer Graphics Forum. p. e15214. Wiley Online Library (2024)
37. Wang, T., Li, M., Zeng, G., Meng, C., Zhang, Q.: Gaussian herding across pens: An optimal transport perspective on global gaussian reduction for 3dgs. In: Advances in Neural Information Processing Systems (NeurIPS 2025) (2025)
38. Wang, Y., Li, Z., Guo, L., Yang, W., Kot, A., Wen, B.: Contextgts: Compact 3d gaussian splatting with anchor level context model. *Advances in neural information processing systems* **37**, 51532–51551 (2024)
39. Wu, G., Yi, T., Fang, J., Xie, L., Zhang, X., Wei, W., Liu, W., Tian, Q., Wang, X.: 4d gaussian splatting for real-time dynamic scene rendering. In: CVPR (2024)
40. Xiong, B., Liu, R., Xu, K., Chen, M., Feng, A.: Splat feature solver. In: ICLR (2026)
41. Yang, Z., Yang, H., Pan, Z., Zhang, L.: Real-time photorealistic dynamic scene representation and rendering with 4d gaussian splatting. In: ICLR (2024)
42. Yang, Z., Gao, X., Zhou, W., Jiao, S., Zhang, Y., Jin, X.: Deformable 3d gaussians for high-fidelity monocular dynamic scene reconstruction. In: CVPR (2024)
43. Yi, T., Fang, J., Wang, J., Wu, G., Xie, L., Zhang, X., Liu, W., Tian, Q., Wang, X.: Gaussiandreamer: Fast generation from text to 3d gaussians by bridging 2d and 3d diffusion models. In: CVPR (2024)
44. Zhang, Y., Jia, W., Niu, W., Yin, M.: Gaussianspa: An "optimizing-sparsifying" simplification framework for compact and high-quality 3d gaussian splatting. In: CVPR (2025)
45. Zhang, Z., Song, T., Lee, Y., Yang, L., Peng, C., Chellappa, R., Fan, D.: Lp-3dgs: Learning to prune 3d gaussian splatting. *Advances in Neural Information Processing Systems* **37**, 122434–122457 (2024)
46. Zhou, J., Fan, L., Chen, X., Huang, L., Liu, S., Li, H.: Gaussianpainter: Painting point cloud into 3d gaussians with normal guidance (2024), <https://arxiv.org/abs/2412.17715>
47. Zhou, S., Chang, H., Jiang, S., Fan, Z., Zhu, Z., Xu, D., Chari, P., You, S., Wang, Z., Kadambi, A.: Feature 3dgs: Supercharging 3d gaussian splatting to enable distilled feature fields. In: CVPR (2024)

# NanoGS: Training-Free Gaussian Splat Simplification

## Supplementary Material

### A Special Case for I Divergence

*Analytical cases and practical estimator.* For two *single* unnormalized Gaussians  $p_i(x) = m_i \mathcal{N}(x | \mu_i, \Sigma_i)$  and  $p_j(x) = m_j \mathcal{N}(x | \mu_j, \Sigma_j)$ , the I-divergence

$$D(p_i \| p_j) = \int \left[ p_i(x) \log \frac{p_i(x)}{p_j(x)} - p_i(x) + p_j(x) \right] dx \quad (12)$$

admits a closed-form expression

$$D(p_i \| p_j) = m_i \left( \log \frac{m_i}{m_j} + \text{KL}(\mathcal{N}_i \| \mathcal{N}_j) \right) - m_i + m_j, \quad (13)$$

where

$$\text{KL}(\mathcal{N}_i \| \mathcal{N}_j) = \frac{1}{2} \left( \text{tr}(\Sigma_j^{-1} \Sigma_i) + (\mu_j - \mu_i)^\top \Sigma_j^{-1} (\mu_j - \mu_i) - d + \log \frac{\det \Sigma_j}{\det \Sigma_i} \right), \quad d = 3. \quad (14)$$

This analytical form is commonly used in Gaussian mixture reduction when both distributions belong to the Gaussian family.

However, the distortion used in our merge criterion compares a *two-component mixture* with a *single Gaussian*:

$$\mathcal{D}_{\text{geo}}(i, j) = \text{KL}(\tilde{p}_{ij} \| q_m), \quad \tilde{p}_{ij}(x) = \pi \mathcal{N}_i(x) + (1 - \pi) \mathcal{N}_j(x), \quad (15)$$

where  $q_m = \mathcal{N}(x; \mu_m, \Sigma_m)$  is the merged Gaussian obtained by moment matching. Because  $\tilde{p}_{ij}$  is a Gaussian *mixture*, the term  $\log(\pi \mathcal{N}_i(x) + (1 - \pi) \mathcal{N}_j(x))$  prevents the integral from admitting a closed-form expression. Consequently, the analytical formulas above cannot be directly applied.

To evaluate the distortion efficiently, we instead approximate the KL divergence using Monte Carlo sampling:

$$\text{KL}(\tilde{p}_{ij} \| q_m) = \mathbb{E}_{x \sim \tilde{p}_{ij}} [\log(\pi \mathcal{N}_i(x) + (1 - \pi) \mathcal{N}_j(x)) - \log q_m(x)]. \quad (16)$$

Given samples  $\{x_s\}_{s=1}^S \sim \tilde{p}_{ij}$ , we estimate

$$\text{KL}(\tilde{p}_{ij} \| q_m) \approx \frac{1}{S} \sum_{s=1}^S [\log(\pi \mathcal{N}_i(x_s) + (1 - \pi) \mathcal{N}_j(x_s)) - \log q_m(x_s)]. \quad (17)$$

Sampling from  $\tilde{p}_{ij}$  is straightforward: we draw from component  $i$  with probability  $\pi$  and from component  $j$  with probability  $1 - \pi$ . In practice we use a small fixed number of samples  $S$  and share common random numbers across candidate pairs to reduce variance while keeping the computation lightweight. This Monte Carlo estimator is the procedure implemented in our codebase.

## B Algorithms

Algorithm 1 describes the greedy KNN edge-collapse procedure used in our implementation. The algorithm takes as input an initial set of splats and a target keep ratio, and progressively reduces the representation through repeated local merges.

The procedure begins with an opacity filtering stage. Since extremely low-opacity splats contribute little to the rendered scene, removing them early improves efficiency and reduces the search space for subsequent merge operations. After this preprocessing step, the algorithm enters an iterative simplification loop.

At each iteration, we build a sparse  $k$ -nearest-neighbor graph over the current splat centers. This graph serves as a locality prior: instead of considering all pairwise combinations, we only evaluate merges between nearby splats. The resulting candidate set is converted into a unique undirected edge list, and each edge is scored by the proposed merge cost. This cost measures how much information would be lost if the two endpoint splats were replaced by a single merged splat.

The core decision step is a greedy disjoint-pair selection. Candidate edges are sorted by increasing cost, and the algorithm scans them in order, selecting an edge whenever neither endpoint has already been assigned in the current pass. This produces a set of non-overlapping merges that can be applied in parallel. The greedy rule is simple but effective: it prioritizes the cheapest local collapses first, while ensuring that the resulting update is consistent.

After the selected pairs are merged, the splat attributes are updated and the algorithm repeats on the new reduced set. Because the KNN graph and edge costs are recomputed after each pass, the method adapts to the evolving geometry of the simplified representation. The loop terminates once the target number of splats is reached or when no further valid merge is available.

Overall, this algorithm can be viewed as a practical graph coarsening strategy for Gaussian splats: the KNN graph defines feasible local collapses, the merge cost ranks them by distortion, and the greedy disjoint matching step realizes a scalable approximation to global simplification.

## C Additional Experiment Results

We provide per-scene quantitative results for all four datasets in Tab. 6, Tab. 3, Tab. 4, and Tab. 5.

In addition to these quantitative results, we also include a demo qualitative video in the supplementary material, which provides further visual comparisons across scenes and compression settings. In the demo video, we also display for large scale out door scene, usually takes about over 10Gb memory, how our compression algorithms perform.

---

**Algorithm 1:** Greedy KNN edge-collapse splat simplification (implementation).

---

**Input:** Input PLY splats  $(\mu, \alpha, s, q, f)$  with  $N_0$  entries; keep ratio  $r \in (0, 1)$ ; KNN size  $k$ ; opacity prune threshold  $\tau$ ; cost params  $cp$ ; edge-cost block size  $B$ .

**Output:** Simplified PLY with  $\approx \lceil rN_0 \rceil$  splats.

Read PLY  $\rightarrow (\mu, \alpha, s, q, f)$ ;  
 $N_0 \leftarrow |\mu|$ ,  $N_{\text{tgt}} \leftarrow \max(\lceil rN_0 \rceil, 1)$ ;  
 $\tau' \leftarrow \min(\tau, \text{median}(\alpha))$ ; // robust prune threshold  
 $\mathcal{I} \leftarrow \{i : \alpha_i \geq \tau'\}$ ; subset  $(\mu, \alpha, s, q, f) \leftarrow (\mu, \alpha, s, q, f)[\mathcal{I}]$ ;  
**while**  $|\mu| > N_{\text{tgt}}$  **do**  
     $N \leftarrow |\mu|$ ;  $k_{\text{eff}} \leftarrow \min(\max(1, k), N - 1)$ ;  
     $\text{nbr} \leftarrow \text{KNN}(\mu, k_{\text{eff}})$ ; // directed  $k$ NN per node  
     $E \leftarrow \text{UNDIRECTEDUNIONEDGES}(\text{nbr})$ ; // unique edges  $\{i, j\}$  with  $i < j$   
     $w \leftarrow \text{EDGECOSTS}(E, \mu, s, q, \alpha, f, cp, B)$ ; // blockwise; uses **fast\_cost\_pairs**  
     $P \leftarrow N - N_{\text{tgt}}$ ; // merges needed this pass  
     $\mathcal{M} \leftarrow \text{GREEDYDISJOINTPAIRS}(E, w, N, P)$ ; // sort by  $w$ , pick **disjoint edges**  
    **if**  $|\mathcal{M}| = 0$  **then**  
        **break**;  
     $(\mu, s, q, \alpha, f) \leftarrow \text{MERGEPAIRS}(\mu, s, q, \alpha, f, \mathcal{M})$ ;  
 $\alpha \leftarrow \text{clip}(\alpha, 0, 1)$ ; write output PLY;

---

## D Generation Results

As stated in the introduction and related work, current 3D Gaussian generation pipelines do not guarantee consistent camera poses or image fidelity. To verify this, we conducted additional experiments on generated data using the following pipeline:

First, we use natural-language prompts to guide mainstream image generation models, such as ChatGPT<sup>3</sup> and Gemini<sup>4</sup>. The resulting images are then used as input for Trellis<sup>5</sup> to generate 3D Gaussian Splats. Finally, we apply our compression method to these assets. The results are illustrated in Fig. 5. The prompts used for 2D image generation can also be multimodal, as shown in Fig. 6.

---

<sup>3</sup> OpenAI, “ChatGPT.” <https://chatgpt.com/> (accessed March 12, 2026).

<sup>4</sup> Google, “Gemini.” <https://gemini.google.com/> (accessed March 12, 2026).

<sup>5</sup> Jianfeng Xiang *et al.*, “Structured 3D Latents for Scalable and Versatile 3D Generation,” in *Proceedings of the IEEE/CVF Conference on Computer Vision and Pattern Recognition (CVPR)*, 2025.

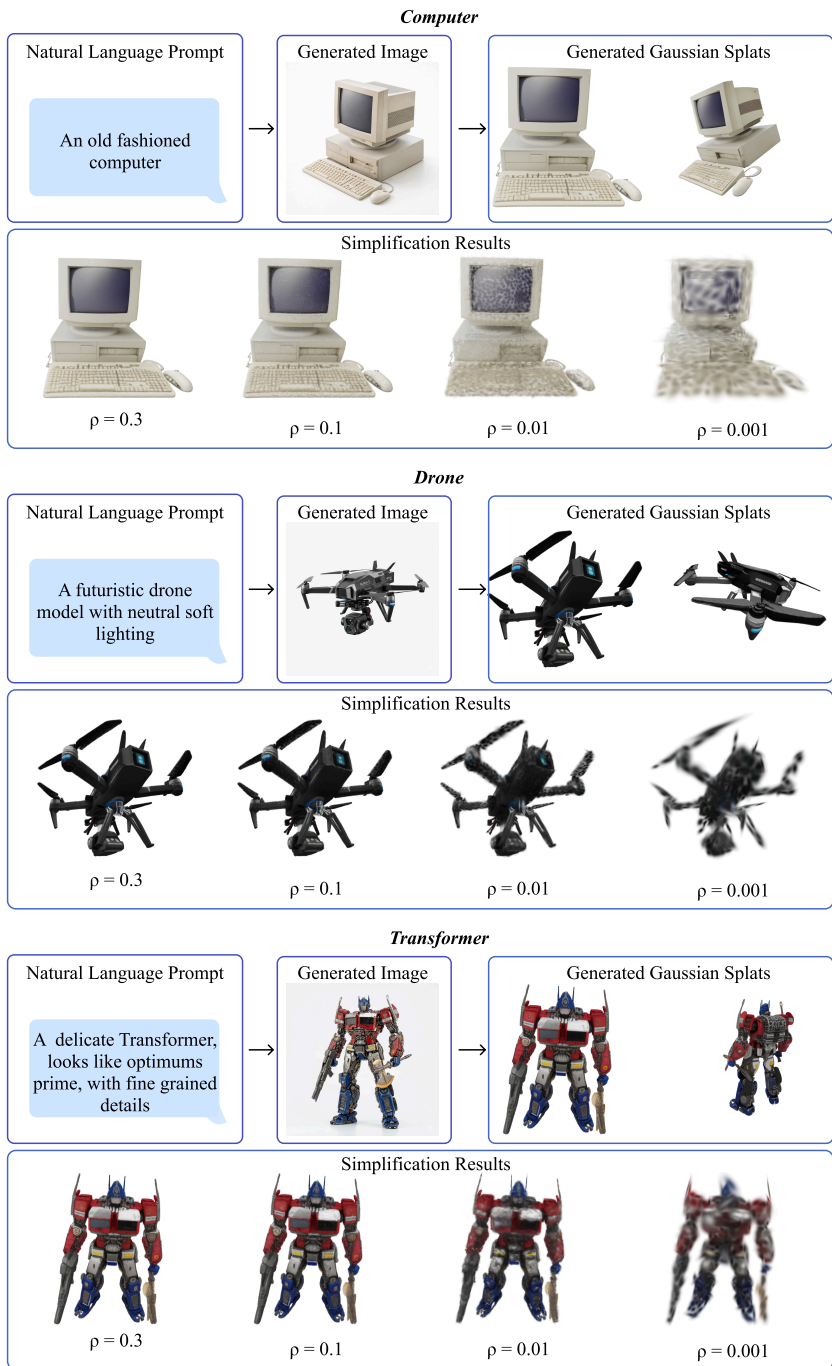


**Fig. 5:** Generated results and corresponding compression results

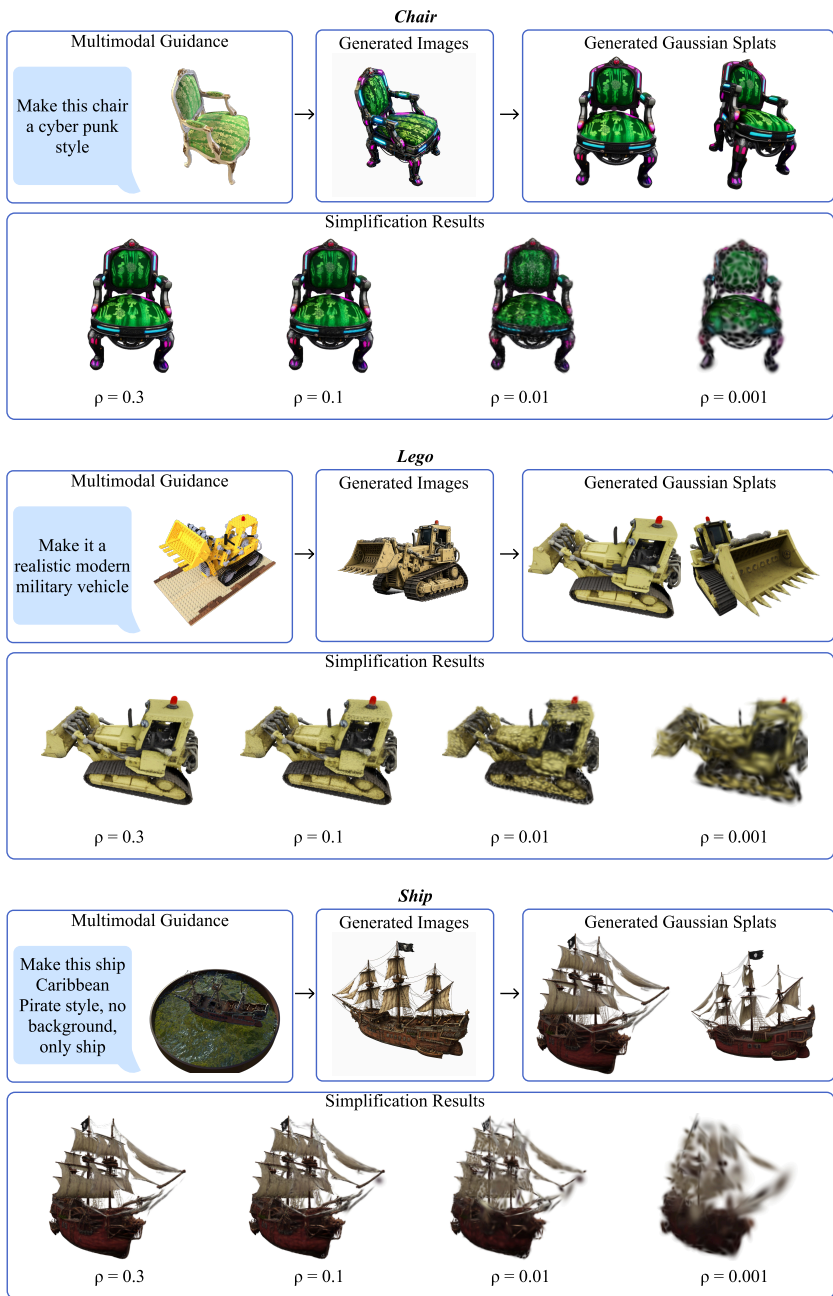


**Fig. 6:** Generated results and corresponding compression results with multimodal inputs

Scene	$\rho = 0.1$			$\rho = 0.01$			$\rho = 0.001$		
	PSNR $\uparrow$	SSIM $\uparrow$	LPIPS $\downarrow$	PSNR $\uparrow$	SSIM $\uparrow$	LPIPS $\downarrow$	PSNR $\uparrow$	SSIM $\uparrow$	LPIPS $\downarrow$
<i>Outdoor Scenes</i>									
bicycle	20.1650	0.4570	0.4558	18.6070	0.3469	0.6292	17.5477	0.3152	0.7256
flowers	17.6026	0.3619	0.5214	16.0689	0.2604	0.6744	14.9127	0.2324	0.7607
garden	21.0113	0.4934	0.4052	19.0978	0.3418	0.5917	16.7483	0.3056	0.7366
stump	21.0693	0.4614	0.4626	19.5957	0.3685	0.6364	18.8344	0.3500	0.7095
treehill	19.0771	0.4168	0.5460	18.0260	0.3766	0.6566	17.0083	0.3608	0.6870
<i>Indoor Scenes</i>									
room	26.1853	0.8025	0.3730	22.3240	0.7219	0.4879	18.3340	0.6526	0.5312
counter	23.5919	0.7390	0.3838	20.2366	0.6447	0.5217	17.0012	0.5884	0.5723
kitchen	24.0360	0.7187	0.3549	19.9008	0.5184	0.5631	17.1972	0.4791	0.6530
bonsai	24.9709	0.7831	0.3849	20.6622	0.6484	0.5192	17.1862	0.5830	0.5716

**Table 3:** Quantitative results for Mip-NeRF 360 dataset across three compaction ratios.

Scene	$\rho = 0.1$			$\rho = 0.01$			$\rho = 0.001$		
	PSNR $\uparrow$	SSIM $\uparrow$	LPIPS $\downarrow$	PSNR $\uparrow$	SSIM $\uparrow$	LPIPS $\downarrow$	PSNR $\uparrow$	SSIM $\uparrow$	LPIPS $\downarrow$
drums	23.5546	0.9139	0.0783	20.6873	0.8580	0.1427	17.4901	0.8112	0.2129
lego	22.5217	0.8791	0.1173	20.4297	0.8036	0.1947	18.1469	0.7763	0.2500
materials	24.2313	0.8992	0.1007	20.5123	0.8360	0.1649	16.6823	0.7926	0.2343
mic	27.5273	0.9632	0.0390	23.8959	0.9291	0.0789	20.4707	0.9014	0.1145
ship	22.3706	0.7958	0.2129	19.4858	0.7432	0.3000	16.3459	0.7061	0.3567
chair	27.2220	0.9256	0.0624	24.0736	0.8772	0.1193	21.7324	0.8554	0.1625
figus	29.4857	0.9634	0.0336	23.6854	0.9105	0.0804	20.6924	0.8656	0.1373
hotdog	29.5549	0.9398	0.0900	25.4385	0.9037	0.1444	20.7310	0.8695	0.1893

**Table 4:** Quantitative results for NeRF Synthetic dataset across three compaction ratios.

Scene	$\rho = 0.1$			$\rho = 0.01$			$\rho = 0.001$		
	PSNR $\uparrow$	SSIM $\uparrow$	LPIPS $\downarrow$	PSNR $\uparrow$	SSIM $\uparrow$	LPIPS $\downarrow$	PSNR $\uparrow$	SSIM $\uparrow$	LPIPS $\downarrow$
truck	19.4503	0.6728	0.3851	16.7092	0.5401	0.5539	14.3262	0.4821	0.6515
train	16.4383	0.5800	0.4416	13.8683	0.4617	0.5975	12.7557	0.4311	0.6304

**Table 5:** Quantitative results for Tanks and Temples dataset across three compaction ratios.

Scene	$\rho = 0.1$			$\rho = 0.01$			$\rho = 0.001$		
	PSNR $\uparrow$	SSIM $\uparrow$	LPIPS $\downarrow$	PSNR $\uparrow$	SSIM $\uparrow$	LPIPS $\downarrow$	PSNR $\uparrow$	SSIM $\uparrow$	LPIPS $\downarrow$
drjohnson	25.5296	0.8241	0.3879	22.7212	0.7618	0.4872	19.6485	0.7265	0.5159
playroom	27.0528	0.8536	0.3545	23.5220	0.7989	0.4473	19.2004	0.7519	0.4986

**Table 6:** Quantitative results for Deep Blending dataset across three compaction ratios.